

MOL #55277

TITLE PAGE

Potential Use of Cetrimonium Bromide as an Apoptosis-Promoting Anti-Cancer Agent for Head and Neck Cancer

Authors:

Emma Ito, Kenneth W. Yip, David Katz, Sonali B. Fonseca, David W. Hedley, Sue Chow, G. Wei Xu, Tabitha E. Wood, Carlo Bastianutto, Aaron D. Schimmer, Shana O. Kelley, and Fei-Fei Liu

Primary Laboratory of Origin

Ontario Cancer Institute, Princess Margaret Hospital
610 University Avenue, Room 7-719
Toronto, Ontario, Canada M5G 2M9

Affiliations:

Department of Medical Biophysics, University of Toronto, Ontario, Canada (*E.I., D.K., D.W.H., S.C., W.X., T.E.W., C.B., A.D.S., F-F.L.*)

Division of Applied Molecular Oncology, Ontario Cancer Institute, University Health Network, Canada (*E.I., D.K., D.W.H., S.C., C.B., F-F.L.*)

Burnham Institute for Medical Research, La Jolla, California (*K.W.Y.*)

Department of Pharmaceutical Sciences, Leslie Dan Faculty of Pharmacy, University of Toronto (*S.B.F., S.O.K.*)

Division of Cancer Genomics and Proteomics, Ontario Cancer Institute, University Health Network (*W.X., T.E.W., A.D.S.*)

Department of Medical Oncology and Hematology, Princess Margaret Hospital, University Health Network (*A.D.S.*)

Department of Biochemistry, Leslie Dan Faculty of Pharmacy, University of Toronto (*S.O.K.*)

Department of Radiation Oncology, Princess Margaret Hospital, University Health Network (*F-F.L.*)

Department of Radiation Oncology, University of Toronto (*F-F.L.*)

RUNNING TITLE PAGE

Running Title:

CTAB: A Mitochondria-Mediated Apoptogenic Agent

Corresponding Author:

Dr. Fei-Fei Liu

Department of Radiation Oncology

Ontario Cancer Institute, Princess Margaret Hospital

Toronto, Ontario, Canada M5G 2M9

Phone: (416) 946-2123

Fax: (416) 946-4586

Email: Fei-Fei.Liu@rmp.uhn.on.ca

Article Format:

Text pages: 24

Tables: 1

Figures: 7

References: 40

Abstract: 216 words

Introduction: 436 words

Discussion: 1500 words

Non-standard Abbreviations:

HTS, high-throughput screen; HNC, head and neck cancer; NPC, nasopharyngeal cancer; RT, radiation therapy; CTAB, cetrimonium bromide; DMSO, dimethyl sulfoxide; CCCP, carbonyl cyanide *m*-chlorophenylhydrazone; Z-VAD.FMK, benzyloxycarbonyl-valine-alanine-aspartate fluoromethylketone; OLIG, oligomycin; NIG, nigericin; MTS, 3-(4,5-dimethylthiazol-2-yl)-5-(3-carboxymethoxyphenyl)-2-(4-sulfophenyl)-2*H*-tetrazolium, inner salt; Gy, gray; DiIC₁(5), 1,1',3,3',3',3'-hexamethylindodicarbocyanine; $\Delta\Psi_M$, mitochondrial membrane potential; JC-1, 5,5',6,6'-tetrachloro-1,1',3,3'-tetraethylbenzimidazolylcarbocyanine iodide; $\Delta\Psi_P$, plasma membrane potential; DiBAC₄(3), bis-(1,3-dibutylbarbituric acid)trimethine oxonol; SCID, severe combined immunodeficient; TLD, tumor-plus-leg diameter; PBS, phosphate-buffered saline; ER, endoplasmic reticulum; PI, propidium iodide; ATPase, ATP synthase; DLC, delocalized lipophilic cation; OXPHOS, oxidative phosphorylation; PTP, mitochondrial permeability transition pore; MOMP, mitochondrial outer membrane permeabilization.

ABSTRACT

A potential therapeutic agent for human head and neck cancer (HNC), cetrimonium bromide (CTAB), was identified through a cell-based phenotype-driven high-throughput screen (HTS) of 2,000 biologically active or clinically used compounds, followed by *in vitro* and *in vivo* characterization of its anti-tumor efficacy. The preliminary and secondary screens were performed on FaDu (hypopharyngeal squamous cancer) and GM05757 (primary normal fibroblasts), respectively. Potential hit compounds were further evaluated for their anti-cancer specificity and efficacy in combination with standard therapeutics on a panel of normal and cancer cell lines. Mechanism of action, *in vivo* anti-tumor efficacy, and potential lead compound optimizations were also investigated. *In vitro*, CTAB interacted additively with γ -radiation and cisplatin, two standard HNC therapeutic agents. CTAB exhibited anti-cancer cytotoxicity against several HNC cell lines, with minimal effects on normal fibroblasts; a selectivity that exploits cancer-specific metabolic aberrations. The central mode of cytotoxicity was mitochondria-mediated apoptosis *via* inhibition of H^+ -ATP synthase activity and mitochondrial membrane potential depolarization, which in turn was associated with reduced intracellular ATP levels, caspase activation, elevated subG₁ cell population, and chromatin condensation. *In vivo*, CTAB ablated tumor-forming capacity of FaDu cells, and delayed growth of established tumors. Thus, using a HTS approach, CTAB was identified as a potential apoptogenic quaternary ammonium compound possessing *in vitro* and *in vivo* efficacy against HNC models.

INTRODUCTION

Head and neck cancer (HNC), which comprises a diverse group of cancers affecting the nasal cavity, sinuses, oral cavity, pharynx, larynx, and other sites in this anatomical region, has an estimated annual global incidence of 533,100 cases (Parkin et al., 2001). It is the fifth most common cancer worldwide with the majority being head and neck squamous cell carcinomas (Jemal et al., 2007; Parkin et al., 2001). Nasopharyngeal cancer (NPC) is a distinct HNC in that 75–81% of NPC patients globally harbor the Epstein-Barr virus (Lo et al., 2004). HNC is a challenging disease due to its heterogeneity and complexity of treatments. Patients with locally advanced disease achieve an overall survival rate of only 50%, despite combined radiation therapy (RT) and chemotherapy treatments, which is unfortunately associated with significant morbidities and toxicities (Rosenthal et al., 2006), underscoring a critical need to develop novel therapeutic strategies to improve clinical outcome.

We have previously developed a rapid, cell-based phenotype-driven high-throughput screen (HTS) for the large-scale identification of novel HNC cytotoxics (Yip et al., 2006a; Yip et al., 2006b). Two existing anti-microbials (benzethonium chloride and alexidine dihydrochloride) were thus identified from the LOPAC1280 and Prestwick chemical libraries. In the current study, the Spectrum Collection small molecule library was screened, identifying cetrimonium bromide (CTAB) as an effective compound against multiple HNC cell lines, with minimal toxicity on normal fibroblasts; a selectivity that appears to exploit cancer-specific metabolic aberrations.

CTAB belongs to a group of quaternary ammonium compounds, which also includes benzethonium chloride and dequalinium chloride, both of which have demonstrated anti-cancer properties *in vitro* and *in vivo* by targeting tumor mitochondria (Bleday et al., 1986; Weiss et al., 1987; Yip et al., 2006b). Quaternary ammonium derivatives have also been reported to show

MOL #55277

enhanced anti-tumor activity compared to their parent compounds (Giraud et al., 2002), suggesting that molecules possessing quaternary ammonium moieties may be highly effective anti-cancer agents.

CTAB is a known component of the broad-spectrum antiseptic cetrimide, which is a mixture of different quaternary ammonium salts that has been clinically used as a tumoricidal irrigant in colorectal cancer surgery (Umpleby and Williamson, 1984), and scolical adjunct to hydatid cyst operations (Sonisik et al., 1998). However, the role of CTAB in cetrimide-mediated anti-microbial and tumoricidal activities has not been investigated extensively; previous studies have in fact described that pure CTAB- and cetrimide-induced anti-microbial effects occur *via* different mechanisms (Smith et al., 1975). To our knowledge, the tumoricidal potential of pure CTAB has not yet been reported, particularly in the context of HNC. This study therefore evaluated the cancer-specific properties of pure CTAB, and assessed its mode of action in HNC models.

MATERIALS AND METHODS

Cell Lines

FaDu (human hypopharyngeal squamous cell cancer), A549 (non-small cell lung adenocarcinoma), MCF7 (breast adenocarcinoma), and MRC5 (normal lung fibroblasts) were obtained from the American Type Culture Collection (Manassas, VA). GM05757 (human primary normal) fibroblasts were obtained from the Coriell Institute for Medical Research (Camden, NJ). All cell lines were cultured according to the manufacturer's specifications. C666-1 (undifferentiated nasopharyngeal cancer) cells (Cheung et al., 1999) were maintained in RPMI 1640 supplemented with 10% fetal bovine serum (Wisent Inc., Quebec, Canada) and antibiotics (100 mg/L penicillin and 100 mg/L streptomycin) as previously described (Yip et al., 2005). UTSCC-8A and -42A (human laryngeal squamous cell cancer) cells were maintained in Dulbecco's modified Eagle's medium supplemented with 10% FBS and antibiotics (100 mg/L penicillin and 100 mg/L streptomycin); UTSCC cells were a gift from R. Grénman (Turku, Finland). All experiments were conducted when cells were in an exponential growth phase.

Small Molecules

The Spectrum Collection (2,000 compounds; MicroSource Discovery Systems, Gaylordsville, CT) was provided by the Samuel Lunenfeld Research Institute High-Throughput Screening Robotics Facility (Toronto, Ontario, Canada). The compounds were initially dissolved using the BioMek FX (Beckman Coulter Inc., Fullerton, CA) in DMSO at a concentration of 10 mM, then diluted in sterile H₂O to 0.1 mM.

Carbonyl cyanide *m*-chlorophenylhydrazone (CCCP) was obtained from Sigma-Aldrich (St. Louis, MO) and dissolved in DMSO (Sigma-Aldrich). The pan-caspase inhibitor, benzyloxycarbonyl-valine-alanine-aspartate fluoromethylketone (Z-VAD.FMK) was purchased

MOL #55277

from BioVision (Mountain View, CA). Oligomycin (Calbiochem, San Diego, CA) and nigericin (Sigma-Aldrich) were dissolved in ethanol with subsequent dilutions prepared in H₂O. Cisplatin (Mayne Pharma-Hospira, Lake Forest, IL), ouabain (Sigma-Aldrich), cetrimonium bromide (Sigma-Aldrich), and all analogues (Alfa Aesar, Ward Hill, MA): cetyltrimethylammonium chloride (analogue 1), dodecyltrimethylammonium bromide (analogue 2), hexyltrimethylammonium bromide (analogue 3), tetramethylammonium bromide (analogue 4), and butyltriethylammonium bromide (analogue 5) were dissolved and diluted in H₂O to the appropriate concentrations. In all cases, the vehicle (untreated) control was H₂O.

Small-Molecule High-Throughput Screening

The BioMek FX and Samuel Lunenfeld Research Institute High-Throughput Screening Robotics platform were used for cell seeding, treatment, and viability assessment as previously described (Yip et al., 2006b). Briefly, FaDu or GM05757 cells were cultured to 85% confluency, trypsinized, and re-suspended in growth media (2.5×10^4 cells/mL). Cells were seeded (5×10^3 /well in 96-well plates) in 200 μ L of growth medium and incubated for 24 hours at 37°C with 5% CO₂ and 95% humidity. Small molecules were then added to a final concentration of 5 μ M. Cells treated with 0.1% DMSO and 166.6 μ M cisplatin were used as negative and positive controls, respectively. After 48 hours, 100 μ L of growth medium was removed from each well. The CellTiter 96 AQueous One Solution Cell Proliferation Assay (3-(4,5-dimethylthiazol-2-yl)-5-(3-carboxymethoxyphenyl)-2-(4-sulfophenyl)-2H-tetrazolium, inner salt; MTS; Promega Corp., Madison, WI) was used to detect cell viability according to the manufacturer's specifications. A 1-hour MTS incubation time was utilized; and 490 nm absorbance was measured on a SpectraMax Plus³⁸⁴ microplate reader (Molecular Devices Corp., Sunnyvale, CA).

Cell Viability Assay

MOL #55277

Cells were seeded (5×10^3 /well in 96-well plates) in 100 μ L of growth medium and incubated for 24 hours at 37°C. The chemicals were then added, to a total volume of 5 μ L. After 48 hours, the MTS assay was performed with DMSO (0.1%)- and cisplatin (166.6 μ M)-treated cells serving as negative and positive controls, respectively.

Colony Formation Assay

Cells were seeded (10^2 – 10^4 /well in 6-well plates) in 3 mL of growth medium and incubated overnight at 37°C. CTAB or vehicle alone (sterile H₂O) was then added at the specified concentrations to a total volume of 50 μ L. After 48 hours, fresh growth medium was added, and the plates were incubated at 37°C. Thirteen days after seeding, colonies were fixed in 70% ethanol, stained with 10% methylene blue, and colonies of ≥ 50 cells were counted. Where indicated, cells were irradiated 24 hours after small-molecule treatment, delivered at room temperature using a ¹³⁷Cs unit (Gammacell 40 Extractor, MDS Nordion, Ottawa, Ontario, Canada) at a dose rate of 1.1 Gy/min.

Fluorescence Microscopy

Cells were seeded (3×10^5 /T-25 flask), incubated for 24 hours, and treated with CTAB (5 μ M; EC₇₅) or vehicle alone at 37°C. After 48 hours, detached and adherent cells were pooled, pelleted at 200 \times g, and stained with 10 μ M Hoechst-33342 (Invitrogen Corp., Carlsbad, CA)-4% formalin-PBS solution. Representative fields were visualized and photographed with a Zeiss Axioskop HBO 40 microscope (Zeiss, Thornwood, NY) under UV illumination.

Caspase Activity Assay

Cells were seeded (4×10^5 /well in 6-well plates), incubated for 24 hours, and treated with CTAB or vehicle alone. Detached and adherent cells were then collected and stained using the CaspGLOW *In Situ* Caspase Staining Kits (BioVision, Mountain View, CA) for caspase-2,

MOL #55277

caspase-3, caspase-8, and caspase-9 activity according to the manufacturer's specifications. Analysis was performed using flow cytometry (FACSCalibur, CellQuest software, Becton Dickinson, San Jose, CA).

Cell Cycle Analysis

Cells were seeded (3×10^5 /T-25 flask), incubated for 24 hours, and treated with CTAB or vehicle alone. Detached and adherent cells were then pooled, pelleted at $200 \times g$, re-suspended in 1.5 mL of hypotonic fluorochrome solution (50 $\mu\text{g/mL}$ propidium iodide, 0.1% sodium citrate, 0.1% Triton X-100; Sigma-Aldrich), and left in the dark at 4°C overnight. Flow cytometric analysis was then performed, and cell cycle distribution was determined using FlowJo software (Tree Star, Inc., San Carlos, CA). Apoptotic cells were defined as cells with DNA content less than G_0/G_1 (hypodiploid).

Transmission Electron Microscopy

Cells were treated with CTAB or vehicle alone and then processed at the University of Toronto, Faculty of Medicine Microscopy Imaging Laboratory (Toronto, Ontario, Canada). Briefly, harvested cells were fixed with Karnosky style fixative (4% paraformaldehyde and 2.5% glutaraldehyde in 0.1 M Sorensen's phosphate buffer, pH 7.2) followed with 1% osmium tetroxide. Cells were then dehydrated with ethanol, washed with propylene oxide, treated with epoxy resin, polymerized at 60°C for 48 hours, sectioned on a Reichert Ultracut E microtome to 80 nm thickness, collected on 300 mesh copper grids, and counterstained with uranyl acetate and lead citrate. Analysis was performed on a Hitachi H7000 transmission electron microscope (Hitachi, Tokyo, Japan) at an accelerating voltage of 75 kV.

Mitochondrial Depolarization, Calcium Content, and Propidium Iodide Uptake

MOL #55277

DiIC₁(5) (1,1',3,3,3',3'-hexamethylindodicarbocyanine; Invitrogen) was used to estimate mitochondrial membrane potential ($\Delta\Psi_M$); cell permeant indo-1 AM (Invitrogen) was used to determine changes in cytosolic calcium, and propidium iodide (Invitrogen) uptake was used to determine cell death as previously described (Schimmer et al., 2001). Briefly, cells were seeded (0.3×10^6 /T-25 flask), incubated for 24 hours, and then treated with CTAB or vehicle alone. Detached and adherent cells were collected, pelleted at $200 \times g$, and re-suspended in medium at a concentration of 10^6 /mL. DiIC₁(5) (40 nM final concentration) and indo-1 AM (2 μ M final concentration) were added to the cell suspensions and incubated at 37°C for 25 minutes, followed by the addition of propidium iodide (1 μ g/mL). Cells were analyzed with a Coulter Epics Elite flow cytometer (Beckman Coulter; DiIC₁(5) excitation 633 nm, 675 ± 20 nm bandpass; indo-1 AM excitation 360 nm, emission ratio 405/525 nm).

Adenosine 5'-Triphosphate (ATP) Synthase Activity Assay

Cells were cultured to confluence in a 15-cm Petri dish and pelleted at $200 \times g$. Fresh mitochondrial ATPase was isolated (130 μ g/reaction), treated with test compounds or vehicle alone, and measured for specific activity using the MitoProfile ATP Synthase Activity/Quantity Rapid Microplate Assay Kit (MitoSciences, Eugene, OR) according to the manufacturer's specifications.

ATP Luminescence Assay

Cells were seeded (5×10^3 /well in 96-well plates) in 200 μ L of growth medium, incubated for 24 hours at 37°C, then treated with CTAB or vehicle alone. Cellular ATP levels were determined using the luciferin-luciferase based ATP Luminescence Assay Kit (Calbiochem) as instructed by the manufacturer.

Plasma and Mitochondrial Membrane Potential Assays

MOL #55277

Cells were seeded (5×10^5 /well in 6-well plates) in 3 mL of growth medium and incubated for 24 hours at 37°C. Mitochondrial membrane potentials were estimated using the MitoProbe JC-1 (5,5',6,6'-tetrachloro-1,1',3,3'-tetraethylbenzimidazolylcarbocyanine iodide) Assay Kit (Invitrogen) according to the manufacturer's specifications. DiBAC₄(3) (bis-(1,3-dibutylbarbituric acid)trimethine oxonol; Invitrogen) was used to estimate relative plasma membrane potentials ($\Delta \Psi_p$). Briefly, detached and adherent cells were collected, pelleted at 200×g, and re-suspended in medium containing 30 nM of DiBAC₄(3). Cells were incubated at 37°C for 30 minutes and washed with PBS. Cells were analyzed with a BD LSR II flow cytometer (BD Biosciences, San Jose, CA; DiBAC₄(3) excitation/emission: 488/516 nm; JC-1 excitation 488 nm, emission ratio 595/526 nm). Data were processed with FACSDiva software (BD Biosciences).

***In Vivo* Tumor Model**

All animal experiments utilized 6 to 8 week-old severe combined immunodeficient (SCID) BALB/c female mice in accordance with the guidelines of the Animal Care Committee, Ontario Cancer Institute, University Health Network (Toronto, Ontario, Canada). The mice were euthanized by CO₂ once tumor-plus-leg diameters (TLD) reached 14 mm. TLD is a well-established tool for assessing *in vivo* therapeutic efficacy and was employed due to the use of intra-muscular tumor models, which are not amenable to 2D-measurements of tumor size.

Tumor Formation Assay

Cells were seeded (2×10^6 /T-75 flask), incubated for 24 hours, and treated as indicated. After 48 hours, cells were harvested and implanted into the left gastrocnemius muscle of SCID mice (2.5×10^5 cells in 100 μ L growth medium per mouse), then monitored for tumor formation by measuring TLDs thrice weekly.

Therapeutic Tumor Growth Assay

The intra-muscular injection of tumor cells into the hind limbs of SCID mice is a well-established method to generate xenograft models to evaluate *in vivo* efficacy and potential toxicities of new therapeutic treatments for HNC, whilst allowing the delivery of local tumor RT (Alajez et al., 2008; Yip et al., 2006b; Yip et al., 2005). Briefly, cells were injected into the left gastrocnemius muscle of SCID mice (2.5×10^5 cells in 100 μ L). Once the TLDs reached an average of 7.5 mm (range 7.25–8.0 mm), mice were randomly assigned to one of the following groups: vehicle, CTAB, RT-plus-vehicle, or RT-plus-CTAB. Mice were administered one intraperitoneal (i.p.) injection (100 μ L bolus) daily of either vehicle (PBS) or CTAB (5 mg/kg dissolved in PBS) for five consecutive days. This dosing regimen was selected based on the CTAB *in vivo* toxicity profiles (Acute Toxicity Determination) provided by the National Cancer Institute/National Institutes of Health Developmental Therapeutics Program *In Vivo* Screening Database (<http://dtp.nci.nih.gov>). A well-tolerated treatment schedule with no evidence of toxicity or lethality in mice was thus selected. Local tumor RT (4 Gy) was delivered on days 2 and 5, immediately prior to the i.p. injections. Briefly, mice were immobilized in a Lucite box and the tumor-bearing leg was exposed to 100 kV (10 mA) at a dose rate of 10 Gy/min, as previously described (Yip et al., 2005). TLDs and body weights were recorded thrice weekly. This drug-plus-RT regimen has been established in our lab as a standard protocol that is generally well tolerated in mice, thereby allowing for direct comparisons of therapeutic efficacy between different experimental intervention strategies *in vivo*.

Statistical Analyses

All experiments were performed at least three independent times, with the data presented as the mean \pm SE. The Z factor was utilized to evaluate the high-throughput screening power

MOL #55277

(Zhang et al., 1999). The statistical differences between treatment groups were determined using the Student's *t* test and one-way ANOVA.

RESULTS

High-Throughput Screening

The preliminary screen of the Spectrum Collection small molecule library (Z factor of 0.73) was conducted on FaDu cells, which represent a clinically relevant model for the study of HNC (Petersen et al., 2005; Zips et al., 2003); the counter-screen was performed on GM05757 fibroblasts due to their ease of manipulation and similar growth kinetics (~20 h doubling-time). Potential hits were defined as compounds that: (a) decreased FaDu cell viability by $\geq 50\%$, but $\leq 10\%$ in GM05757 fibroblasts or (b) induced >3 -fold reduction in FaDu viability compared to GM05757. Eighteen compounds were thus identified to demonstrate preferential toxicity against FaDu cells (Table 1), ranging in function from anti-microbial, apoptosis-promoting, anti-metabolite, to DNA alkylation. The validity of the screen was corroborated by the identification of existing chemotherapeutic agents such as novantrone, dactinomycin, and mechlorethamine, as well as the two recently described anti-cancer agents (Yip et al., 2006a; Yip et al., 2006b). Amongst the 18 hits, only one compound, cetrimonium bromide (Fig. 1A), was identified with heretofore-unreported tumoricidal properties against HNC; hence, selected for further evaluation.

Validation of HTS Hits and Evaluation of Anti-Cancer Specificity

A dose-response evaluation of CTAB on six cancer and two normal cell lines was performed to confirm the initial high-throughput screening results, and to further assess its anti-cancer potential. HNC is a highly heterogeneous disease; hence, we selected cell line models representing that spectrum, ranging from nasopharyngeal, laryngeal, to hypopharyngeal subsites. The effective concentration required to reduce cell viability by 50% after 48 hours of treatment (EC_{50}) was $\sim 2 \mu\text{M}$ in FaDu, $\sim 3.8 \mu\text{M}$ in C666-1, $\sim 3.5 \mu\text{M}$ in UTSCC-8A, and $\sim 4.2 \mu\text{M}$ in UTSCC-42A cells (Fig. 1B). In contrast, the EC_{50} values were much higher in normal cells; ~ 11

μM in MRC5 and $\sim 18 \mu\text{M}$ in GM05757 fibroblasts. Furthermore, the other human cancer models demonstrated differential sensitivity with higher EC_{50} values of $\sim 17 \mu\text{M}$ for A549 lung and $\sim 12 \mu\text{M}$ for MCF7 breast cancer cells. Subsequent studies focused primarily on FaDu cells, the most CTAB-sensitive cancer cell line.

Evaluation of Combination Therapy

To evaluate the effect of combining CTAB with traditional HNC therapeutics, FaDu cells were exposed to increasing concentrations of CTAB combined with γ -radiation or cisplatin. The clonogenic survival curves demonstrated that CTAB interacted additively with radiation in a dose-dependent manner (Fig. 1C), similar to the effect observed with cisplatin (data not shown).

Cetrimonium Bromide Induces Apoptosis

In an effort to elucidate the mode of cell death induced by CTAB in HNC, apoptosis and cell cycle analyses were conducted. Hoechst-33342 staining of FaDu cells treated with CTAB revealed nuclear condensation and blebbing, consistent with apoptotic nuclear morphology, which was not observed in CTAB-treated GM05757 fibroblasts (Fig. 2A). Flow cytometric DNA content analyses also revealed a dramatic increase in the population of FaDu and C666-1 cells with subG₁ DNA content, but not for the GM05757 fibroblasts (Fig. 2B). On the other hand, cell cycle arrest was not detected in either HNC cell line (data not shown). CTAB-induced caspase activation was also evaluated in cells treated for 6, 12, 24, 48, 72, 96, or 120 hours (Fig. 2C, not all data shown). Activation of the caspase cascade, a hallmark of apoptosis, was observed as early as 12 hours in CTAB-treated FaDu and C666-1 cells, and continued to increase in a time-dependent manner; in contrast to minimal activation in the GM05757 fibroblasts. The use of a pan-caspase inhibitor, Z-VAD.FMK, revealed CTAB-induced cytotoxicity to be highly dependent on caspase activation (Fig. 2D).

MOL #55277

Transmission electron microscopy was utilized to better define the subcellular morphological characteristics of apoptosis, such as chromatin condensation and membrane blebbing. Progressive morphologic abnormalities in the mitochondria were observed after 24, 48, or 96 hours of CTAB treatment in FaDu cells (Fig. 3A), but not in GM05757 fibroblasts (Fig. 3B); the rough endoplasmic reticulum (ER) remained relatively intact.

To further investigate the mechanism of apoptosis in CTAB-mediated cell death, cytosolic calcium increase, which may result from damage of the ER or Ca^{2+} plasma membrane channels, as well as mitochondrial membrane potential depolarization, which has been hypothesized to be a marker of apoptotic cells (Ferri and Kroemer, 2001), were evaluated. The proportion of FaDu cells with depolarized mitochondria increased with longer treatment times (1.5% at 2 h, 4.4% at 4 h, 11.4% at 6 h, and 24.2% at 12 h, *vs.* 1.2% at 12 h with vehicle alone; Fig. 3C, box A). Furthermore, increased cytosolic Ca^{2+} levels could be observed in cells with depolarized mitochondria. Loss of membrane integrity and cell death, indicated by propidium iodide (PI) uptake, also increased with incubation time (0.4% at 2 h, 2.5% at 4 h, 6.8% at 6 h, and 11.7% at 12 h, *vs.* 0.3% at 12 h with vehicle alone; Fig. 3C, box C). The presence of a cell population with decreased $\Delta\Psi_{\text{M}}$ that excluded PI (Fig. 3C, box D) confirmed that the collapse of $\Delta\Psi_{\text{M}}$ was a primary cellular event leading to cell death.

Cetrimonium Bromide Perturbs Mitochondrial Function

CTAB has previously been reported to compromise bioenergetic homeostasis by inhibiting H^{+} -ATP synthase (Barzu et al., 1989). To determine if CTAB induced apoptosis in HNC cells *via* inhibition of ATP synthase (ATPase), freshly isolated mitochondria were solubilized, treated with CTAB, and monitored for enzymatic activity. CTAB reproducibly decreased ATPase activity in a dose-dependent manner; achieving ~90% inhibition at 50 μM

(Fig. 4A). The extent of inhibition by CTAB was comparable to that of oligomycin, a potent mitochondrial H^+ -ATP synthase inhibitor. Ouabain, a selective Na^+/K^+ -ATPase inhibitor had minimal effect on ATPase activity, validating the specificity of H^+ -ATPase inhibition by CTAB.

The inhibition of mitochondrial H^+ -ATPase should lead to a progressive reduction in intracellular ATP levels; this was indeed observed after 12 hours of CTAB exposure, which caused a modest (~10%), but statistically significant decrease in ATP content in FaDu cells (Fig. 4B). However, by 24 hours, total intracellular ATP level fell to ~12%, and continued to decline in a time-dependent manner. In contrast, ATP levels in GM05757 fibroblasts were minimally perturbed.

Role of $\Delta\Psi_M$ in Cetrimonium Bromide-Mediated Cell Death

Previous findings have suggested that the composition and function of mitochondria in cancer and normal cells differ, including a higher $\Delta\Psi_M$ (Fantin and Leder, 2006). Hence, the relative intrinsic mitochondrial transmembrane potentials of GM05757, MRC5, A549, and FaDu cells were measured, demonstrating that FaDu cells had the highest $\Delta\Psi_M$ compared to the low values for both types of fibroblasts, with an intermediate value for A549 cells (Fig. 5A). This relative difference in $\Delta\Psi_M$ reflects the respective differential sensitivity to CTAB (Fig. 1B).

To further investigate the determinative role of $\Delta\Psi_M$ in CTAB-mediated cell death, FaDu cells were pre-incubated with CCCP, a protonophore that dissipates the proton gradient; a low concentration of CCCP was used to effectively uncouple $\Delta\Psi_M$, without perturbing $\Delta\Psi_P$ (Fig. 5B). Mild $\Delta\Psi_M$ uncoupling prior to CTAB treatment significantly suppressed CTAB-induced apoptosis by >50% (Fig. 5C). In comparison, oligomycin, another potent ATPase inhibitor (Fig. 4A), did not respond to changes in $\Delta\Psi_M$ (Fig. 5D) and demonstrated no selective cytotoxicity

amongst the different cancer cell lines tested (Fig. 5E); an observation that was expected since oligomycins are neutral macrolide antibiotics that could induce cell death independent of $\Delta\psi_M$.

To examine the involvement of the electrochemical pH-gradient in CTAB-mediated apoptosis, FaDu cells were pre-treated with nigericin, a K^+/H^+ exchange ionophore that dissipates the pH gradient across the mitochondrial membrane. Perturbing the pH gradient prior to CTAB treatment did not protect against cytotoxicity (Fig. 5F). In fact, a modest dose-dependent increase in apoptosis was observed, corresponding to the compensatory increase in $\Delta\psi_M$ that is anticipated with a pH gradient loss (Davis et al., 1985), which in turn could enhance CTAB accumulation within the mitochondria.

Elimination of Tumor Formation

To evaluate the effect of CTAB on tumorigenesis *in vivo*, FaDu cells treated with CTAB (EC_{75}) were injected into the left gastrocnemius muscle of SCID mice (2.5×10^5 cells/mouse); establishing a three-dimensional system that simulates the complex tumor micro-environment. Mice implanted with CTAB-treated FaDu cells did not develop tumors even after 100 days (Fig. 6A). In contrast, mice with vehicle-treated cells (implanted with 6.25×10^4 cells, representing the proportion of viable cells post-treatment with EC_{75}), developed tumors as early as 15 days, clearly demonstrating that CTAB effectively eliminated the tumor-forming potential of FaDu cells in SCID mice.

Growth Delay in Established Xenograft Tumors

The therapeutic efficacy of CTAB in treating established FaDu xenograft tumors in SCID mice was also evaluated. Once the TLDs reached an average of 7.5 mm, the mice were treated with CTAB (daily 5 mg/kg i.p. for 5 days). The dosing regimen was not optimized for absorption, distribution, metabolism, or excretion, but a delay in tumor growth (i.e. therapeutic

MOL #55277

benefit) was nonetheless observed. CTAB induced a modest reduction in tumor development compared to the vehicle-treatment arm; delaying the mean time to reach a TLD of 14 mm by ~3.7 days ($P < 0.05$; Fig. 6B). When combined with local tumor RT, CTAB appeared to have a modest additive effect by extending the mean time to reach 14 mm by ~7.2 days ($P < 0.05$; Fig. 6B). These data strongly suggest that improving the pharmacokinetics and bioavailability of CTAB would render this compound highly effective; as the *in vivo* tumor-forming capacity of FaDu cells was completely ablated when every tumor cell was exposed to the drug (Fig. 6A).

***In Vivo* Safety and Toxicity**

To assess the *in vivo* safety and toxicity of our CTAB dosing regimen (~0.05% i.p.), the body weights of tumor-bearing mice were monitored. The four treatment groups exhibited no significant difference in overall body weight (Fig. 6C), indicating that this treatment was well tolerated, as no evidence of toxicity or lethality was observed.

Evaluation of Cetrimonium Bromide Analogues

To explore the structure-function relationship of CTAB with a focus on understanding the importance of its chain length, five commercially available analogues were evaluated on FaDu and GM05757 cells (Fig. 7A). Substitution of Br^- with Cl^- did not significantly diminish the inhibitory actions of the compound (analogue 1). Complete removal of the alkyl chain however, abolished any anti-cancer activity (analogue 4). Derivatives with carbon chains $\text{C}_n < 12$ demonstrated a complete loss of inhibition (analogues 3–5); as did the sterically bulky quaternary ammonium group of analogue 5. Only analogues 1 (cetyltrimethylammonium chloride) and 2 (dodecyltrimethylammonium bromide) retained cytotoxicity and bioactivity with EC_{50} values similar to those measured for CTAB: 2.5 μM vs. 14 μM for analogue 1, and 4 μM vs. 30 μM for analogue 2, in FaDu and GM05757 cells, respectively (Figs. 7B and C).

DISCUSSION

In the current study, a phenotype-driven HTS of the Spectrum Collection small molecule library was performed for the large-scale identification of novel HNC cytotoxics. Cetrimonium bromide, an existing anti-microbial (Pang and Willis, 1997), was identified to have anti-cancer efficacy against several human HNC cell lines with minimal toxicity towards normal cells. Our data document CTAB to significantly compromise mitochondrial bioenergetic function, inducing cell death primarily through the intrinsic caspase-dependent apoptotic pathway; non-apoptotic death such as senescence and mitotic catastrophe were not observed (data not shown). FaDu cells, which represent a highly aggressive HNC cell line, sustained sufficient damage upon CTAB treatment to irreversibly inhibit the clonal growth of cultured carcinoma cells *in vitro*, and ablate tumorigenicity *in vivo*. When combined with local RT, CTAB delayed tumor growth whilst maintaining a favorable toxicity profile. CTAB is a known component of cetrimide, which has been routinely used during hydatid cyst, and colorectal surgeries at concentrations that are clinically well tolerated. In rare cases, cardiac ischemia, chemical peritonitis, and methemoglobinemia have been reported with cetrimide concentrations ranging from ~1–5% (Gilchrist, 1979; Pang and Willis, 1997); 12% cetrimide solutions found in common household products have been occasionally associated with erythema and skin blistering (Inman, 1982). No clinical case reports of toxicity have been described relating to administration of pure CTAB. Nonetheless, the CTAB dosing utilized in our study was well tolerated in the treated mice, with good maintenance of their body weights.

CTAB is a quaternary ammonium compound, belonging to a group of small molecules, known as delocalized lipophilic cations (DLCs). Due to their lipophilic nature and delocalized positive charge, DLCs can penetrate the hydrophobic barriers of plasma and mitochondrial

MOL #55277

membranes, and accumulate in the mitochondria in response to the negative transmembrane potential, resulting in mitochondriotoxicity (Chen, 1988). Accordingly, the determinative role of $\Delta\Psi_M$ in CTAB-mediated cytotoxicity was demonstrated as mild $\Delta\Psi_M$ uncoupling prior to CTAB treatment significantly suppressed the overall level of apoptosis in FaDu cells (Fig. 5C); while perturbation of the mitochondrial pH gradient and corresponding compensatory $\Delta\Psi_M$ increase *via* nigericin enhanced CTAB-induced apoptosis (Fig. 5F).

Dysregulation of mitochondrial functions and aberrant metabolic bioenergetics are mechanisms cancer cells have developed to resist mitochondrial-mediated apoptosis, thereby surviving in the toxic tumor micro-environment (Kroemer, 2006). These features however, can be exploited for the development of novel anti-cancer therapies targeting mitochondrial proteins and membranes to promote cell death. Elevated intrinsic plasma and/or mitochondrial membrane potentials have been reported for various cancer cells (Dairkee and Hackett, 1991; Davis et al., 1985; Heerdt et al., 2005); with higher $\Delta\Psi_M$ attributed to the buildup of the mitochondrial proton gradient, resulting from reduced oxidative phosphorylation (OXPHOS) (Chen, 1988; Warburg, 1930). Such $\Delta\Psi_M$ differences of >60 mV can therefore result in a >10-fold accumulation of DLCs in tumor *vs.* normal mitochondria (Modica-Napolitano and Aprille, 1987).

The degree of glycolytic up-regulation also varies between different tumors, which might in part explain the differential sensitivity to CTAB amongst the various cancer cell lines. Head and neck cancers, which are often hypoxic, are commonly associated with high aerobic glycolytic activity and increased aggressiveness (Cohen et al., 2004; Isa et al., 2006); while the MCF7 breast and A549 lung cancer cells have relatively lower aerobic glucose consumption rates (Robey et al., 2005). Accordingly, we observed A549 cells to have lower intrinsic $\Delta\Psi_M$ than FaDu cells (Fig. 5A); correlating with their relative cytotoxicity profiles (Fig. 1B). Taken

together, the basis of selectivity of CTAB against HNC cells appears to be rooted at the mitochondrial level, with subtle differences in $\Delta\Psi_M$ being a key regulator. Thus, CTAB would be predicted to be more effective against tumors that rely heavily on glycolysis, and are dependent on the Warburg effect.

Once CTAB is concentrated into the tumor mitochondria, the H^+ -gradient across the inner mitochondrial membrane may begin to dissipate, with the consequent $\Delta\Psi_M$ decline sensed by the mitochondrial permeability transition pore (PTP) (Scorrano et al., 1997). Opening of the PTP causes mitochondrial outer membrane permeabilization (MOMP), a pivotal event in the intrinsic apoptotic pathway, leading to the disruption of essential mitochondrial functions, along with release of apoptogenic factors, such as cytochrome c (Green and Kroemer, 2004). We detected $\Delta\Psi_M$ depolarization as early as 2 hours post-treatment (Fig. 3C) with caspase-9 activation after 12 hours (Fig. 2C), indicating that mitochondrial damage is an early event in CTAB-induced cell death. Structural abnormalities observed at 24 hours (Fig. 3A) may represent dysfunctional mitochondria that are being eliminated *via* autophagy (Kundu and Thompson, 2005). The high levels of initiator caspase-9 activation (Fig. 2C) suggest that mitochondria-mediated apoptosis may be the primary mechanism by which CTAB exerts its cytotoxic effect.

Increased cytosolic Ca^{2+} levels were also detected in cells with depolarized mitochondria, which may be associated with endoplasmic reticulum Ca^{2+} release during ER-stress induced apoptosis. Increased cytosolic Ca^{2+} can trigger mitochondrial Ca^{2+} overload, resulting in $\Delta\Psi_M$ collapse, with subsequent MOMP and cytochrome c release, thereby activating the caspase cascade (Xu et al., 2005). The activation of initiator caspases-2 and -8, which was observed to a lesser extent in CTAB-treated HNC cells (Fig. 2C), is also involved in the ER-stress response

(Momoi, 2004; Xu et al., 2005). Collectively, this suggests that activation of both ER- and mitochondria-mediated apoptotic pathways is responsible for CTAB-induced cytotoxicity.

We and others (Barzu et al., 1989) have demonstrated that CTAB compromises mitochondrial bioenergetic regulation *via* inhibition of ATP synthase, which consists of the membrane-embedded F_0 (H^+ -translocation) and peripheral catalytic F_1 (ATP synthesis/hydrolysis) subcomplexes (Capaldi and Aggeler, 2002). The ATPase couples the electrochemical H^+ -gradient to ATP synthesis/hydrolysis and is responsible for maintaining the $\Delta \Psi_M$ in response to changes in the proton motive force (Capaldi and Aggeler, 2002; Suzuki et al., 2003). Thus, mitochondrial repolarization *via* ATP hydrolysis may occur to counteract the CTAB-induced depolarization in cancer cells. The ability of CTAB to directly bind and inhibit ATPase will prevent $\Delta \Psi_M$ repolarization, serving as another means of committing cancer cells to death. It should be noted that the CTAB concentrations required to significantly inhibit ATPase activity were higher than the cytotoxic doses in FaDu cells (Figs. 4A and 1B). Previous studies have observed that higher levels of CTAB are necessary to inhibit the activity of purified ATPase *vs.* the enzyme in the presence of sub-mitochondrial particles (membrane-bound ATPase) (Barzu et al., 1989), which could potentially explain the difference in concentrations. In comparison, the neutrally charged oligomycin, which was unresponsive to subtle $\Delta \Psi_M$ changes (Fig. 5D), and thus demonstrated no selective cytotoxicity amongst different cancer cell lines (Fig. 5E), was able to inhibit ATPase at concentrations much lower than its cytotoxic doses (Figs. 4A and 5E). Thus, CTAB-induced cell death involves, at least in part, ATPase inhibition, although this might not be its primary mode of action.

Since mitochondria-mediated cytotoxicity is complex, and can proceed simultaneously *via* multiple mechanisms, additional mitochondriotoxic effects cannot be ruled out. The

MOL #55277

preliminary biological action of cationic CTAB may be the $\Delta\Psi_M$ -driven accumulation in the tumor mitochondria, initiating a multitude of secondary effects ($\Delta\Psi_M$ depolarization, lipid peroxidation, ATPase inhibition, etc.) that collectively perturb mitochondrial function and ultimately, induce apoptosis. The CTAB-induced onion-skin appearance of damaged mitochondria (Fig. 3A) is consistent with lipid peroxidation, which has also been reported with other DLCs *via* membrane intercalation and reactive oxygen species, resulting in membrane permeabilization (Modica-Napolitano et al., 1998; Modica-Napolitano et al., 1996). Thus, the possibility of CTAB promoting membrane lipid peroxidation also warrants further evaluation.

Interestingly, CTAB has recently been implicated in the regulation of OXPHOS expression (Wagner et al., 2008), whereby it decreased the transcription of nuclear-encoded OXPHOS genes, including *atp5a1*, *atp5c1*, and *atp5o*, all of which encode subunits of the ATPase F₁ complex. Furthermore, CTAB has been shown to specifically interact with negatively charged acidic residues buried in the hydrophobic environments of the F₁ moiety (Barzu et al., 1989). These findings point towards a unique mechanism by which CTAB appears to be able to down-regulate the transcription of certain ATPase subunits, as well as physically inhibit their enzymatic activities.

The desirable anti-cancer activity of CTAB suggests that analogues based on structural modification may result in more efficacious lead compounds. As such, commercially available derivatives were exploited to examine the structure-function relationship of CTAB. Our results indicate that the combination of both the positively charged quaternary nitrogen and non-polar hydrophobic alkyl chain are indispensable for its cytotoxic effect. This inhibitory action also appeared to be highly dependent on the length of the alkyl chain, as analogues with shorter tails exhibited reduced cytotoxicity. Additional testing of cetrimonium analogues with longer alkyl

MOL #55277

chains may provide useful starting points for further lead optimization. Taken together, our results suggest that the positively charged polar head of CTAB provides the basis for its anti-cancer specificity, while the non-polar hydrophobic tail may aid in its insertion into the plasma membrane. The lipophilic nature, delocalized positive charge, and structural similarity to sphingosine, a primary component of sphingolipids, may allow CTAB to readily penetrate the hydrophobic barriers of the lipid bilayer and accumulate within the tumor cell.

In conclusion, we have identified CTAB as a clinically relevant, novel anti-cancer agent for HNC. P53 is mutated in over ~50% of human cancers (Hainaut et al., 1997) and is correlated with poor prognosis and enhanced resistance to commonly used chemotherapeutic agents (Breen et al., 2007). Examination of CTAB-treated wild-type ($p53^{+/+}$) and mutant ($p53^{-/-}$) colon cancer HCT116 cells (Bunz et al., 1998) demonstrated very similar sensitivity (data not shown), suggesting that CTAB-mediated toxicity is independent of p53 status; thereby increasing the potential applicability of CTAB to many different human cancers. Moreover, its favorable toxicity profile, ability to induce apoptosis in cancer cells at much lower concentrations than its anti-microbial application (Pang and Willis, 1997), and capacity to delay tumor growth in FaDu xenograft models comparable to paclitaxel (Davis et al., 2002), a commonly used chemotherapeutic agent in the clinical management of HNC patients (Agarwala et al., 2007), all suggest that optimizing the bio-availability and pharmacokinetics of CTAB could provide an exciting opportunity for the development of a highly effective drug candidate, capable of exploiting the metabolic aberrations of human head and neck cancers.

MOL #55277

ACKNOWLEDGMENTS

We thank Alessandro Datti, Thomas Sun, and Frederick Vizeacoumar from the Samuel Lunenfeld Research Institute High-Throughput Screening Robotics Facility for their assistance with the high-throughput screen.

REFERENCES

- Agarwala SS, Cano E, Heron DE, Johnson J, Myers E, Sandulache V, Bahri S, Ferris R, Wang Y, and Argiris A (2007) Long-term outcomes with concurrent carboplatin, paclitaxel and radiation therapy for locally advanced, inoperable head and neck cancer. *Ann Oncol* **18**:1224-1229.
- Alajez NM, Mocanu JD, Shi W, Chia MC, Breitbach CJ, Hui AB, Knowles S, Bell JC, Busson P, Takada K, Lo KW, O'Sullivan B, Gullane P, and Liu FF (2008) Efficacy of systemically administered mutant vesicular stomatitis virus (VSVDelta51) combined with radiation for nasopharyngeal carcinoma. *Clin Cancer Res* **14**:4891-4897.
- Barzu O, Guerrieri F, Scarfo R, Capozza G, and Papa S (1989) Effect of cetyltrimethylammonium on ATP hydrolysis and proton translocation in the F₀-F₁ H⁺-ATP synthase of mitochondria. *J Bioenerg Biomembr* **21**:403-414.
- Bleday R, Weiss MJ, Salem RR, Wilson RE, Chen LB, and Steele G, Jr. (1986) Inhibition of rat colon tumor isograft growth with dequalinium chloride. *Arch Surg* **121**:1272-1275.
- Breen L, Heenan M, Amberger-Murphy V, and Clynes M (2007) Investigation of the role of p53 in chemotherapy resistance of lung cancer cell lines. *Anticancer Res* **27**:1361-1364.
- Bunz F, Dutriaux A, Lengauer C, Waldman T, Zhou S, Brown JP, Sedivy JM, Kinzler KW, and Vogelstein B (1998) Requirement for p53 and p21 to sustain G2 arrest after DNA damage. *Science* **282**:1497-1501.
- Capaldi RA, and Aggeler R (2002) Mechanism of the F(1)F(0)-type ATP synthase, a biological rotary motor. *Trends Biochem Sci* **27**:154-160.
- Chen LB (1988) Mitochondrial membrane potential in living cells. *Annu Rev Cell Biol* **4**:155-181.

MOL #55277

- Cheung ST, Huang DP, Hui AB, Lo KW, Ko CW, Tsang YS, Wong N, Whitney BM, and Lee JC (1999) Nasopharyngeal carcinoma cell line (C666-1) consistently harbouring Epstein-Barr virus. *Int J Cancer* **83**:121-126.
- Cohen NA, Lai SY, Ziober AF, and Ziober BL (2004) Dysregulation of hypoxia inducible factor-1alpha in head and neck squamous cell carcinoma cell lines correlates with invasive potential. *Laryngoscope* **114**:418-423.
- Dairkee SH, and Hackett AJ (1991) Differential retention of rhodamine 123 by breast carcinoma and normal human mammary tissue. *Breast Cancer Res Treat* **18**:57-61.
- Davis PD, Dougherty GJ, Blakey DC, Galbraith SM, Tozer GM, Holder AL, Naylor MA, Nolan J, Stratford MR, Chaplin DJ, and Hill SA (2002) ZD6126: a novel vascular-targeting agent that causes selective destruction of tumor vasculature. *Cancer Res* **62**:7247-7253.
- Davis S, Weiss MJ, Wong JR, Lampidis TJ, and Chen LB (1985) Mitochondrial and plasma membrane potentials cause unusual accumulation and retention of rhodamine 123 by human breast adenocarcinoma-derived MCF-7 cells. *J Biol Chem* **260**:13844-13850.
- Fantin VR, and Leder P (2006) Mitochondriotoxic compounds for cancer therapy. *Oncogene* **25**:4787-4797.
- Ferri KF, and Kroemer G (2001) Organelle-specific initiation of cell death pathways. *Nat Cell Biol* **3**:E255-263.
- Gilchrist DS (1979) Chemical peritonitis after cetrime washout in hydatid-cyst surgery. *Lancet* **2**:1374.
- Giraud I, Rapp M, Maurizis JC, and Madelmont JC (2002) Synthesis and in vitro evaluation of quaternary ammonium derivatives of chlorambucil and melphalan, anticancer drugs designed for the chemotherapy of chondrosarcoma. *J Med Chem* **45**:2116-2119.

- Green DR, and Kroemer G (2004) The pathophysiology of mitochondrial cell death. *Science* **305**:626-629.
- Hainaut P, Soussi T, Shomer B, Hollstein M, Greenblatt M, Hovig E, Harris CC, and Montesano R (1997) Database of p53 gene somatic mutations in human tumors and cell lines: updated compilation and future prospects. *Nucleic Acids Res* **25**:151-157.
- Heerdt BG, Houston MA, and Augenlicht LH (2005) The intrinsic mitochondrial membrane potential of colonic carcinoma cells is linked to the probability of tumor progression. *Cancer Res* **65**:9861-9867.
- Inman JK (1982) Cetrimide allergy presenting as suspected non-accidental injury. *Br Med J (Clin Res Ed)* **284**:385.
- Isa AY, Ward TH, West CM, Slevin NJ, and Homer JJ (2006) Hypoxia in head and neck cancer. *Br J Radiol* **79**:791-798.
- Jemal A, Siegel R, Ward E, Murray T, Xu J, and Thun MJ (2007) Cancer statistics, 2007. *CA Cancer J Clin* **57**:43-66.
- Kroemer G (2006) Mitochondria in cancer. *Oncogene* **25**:4630-4632.
- Kundu M, and Thompson CB (2005) Macroautophagy versus mitochondrial autophagy: a question of fate? *Cell Death Differ* **12 Suppl 2**:1484-1489.
- Lo KW, To KF, and Huang DP (2004) Focus on nasopharyngeal carcinoma. *Cancer Cell* **5**:423-428.
- Modica-Napolitano JS, and Aprille JR (1987) Basis for the selective cytotoxicity of rhodamine 123. *Cancer Res* **47**:4361-4365.
- Modica-Napolitano JS, Brunelli BT, Koya K, and Chen LB (1998) Photoactivation enhances the mitochondrial toxicity of the cationic rhodacyanine MKT-077. *Cancer Res* **58**:71-75.

- Modica-Napolitano JS, Koya K, Weisberg E, Brunelli BT, Li Y, and Chen LB (1996) Selective damage to carcinoma mitochondria by the rhodacyanine MKT-077. *Cancer Res* **56**:544-550.
- Momoi T (2004) Caspases involved in ER stress-mediated cell death. *J Chem Neuroanat* **28**:101-105.
- Pang S, and Willis L (1997) Final report on the safety assessment of cetrimonium chloride, cetrimonium bromide, and steatrimonium chloride. *Int J Toxicol* **16**:195-220.
- Parkin DM, Bray F, Ferlay J, and Pisani P (2001) Estimating the world cancer burden: Globocan 2000. *Int J Cancer* **94**:153-156.
- Petersen C, Zips D, Krause M, Volkel W, Thames HD, and Baumann M (2005) Recovery from sublethal damage during fractionated irradiation of human FaDu SCC. *Radiother Oncol* **74**:331-336.
- Robey IF, Lien AD, Welsh SJ, Baggett BK, and Gillies RJ (2005) Hypoxia-inducible factor-1alpha and the glycolytic phenotype in tumors. *Neoplasia* **7**:324-330.
- Rosenthal DI, Lewin JS, and Eisbruch A (2006) Prevention and treatment of dysphagia and aspiration after chemoradiation for head and neck cancer. *J Clin Oncol* **24**:2636-2643.
- Schimmer AD, Hedley DW, Chow S, Pham NA, Chakrabartty A, Bouchard D, Mak TW, Trus MR, and Minden MD (2001) The BH3 domain of BAD fused to the Antennapedia peptide induces apoptosis via its alpha helical structure and independent of Bcl-2. *Cell Death Differ* **8**:725-733.
- Scorrano L, Petronilli V, and Bernardi P (1997) On the voltage dependence of the mitochondrial permeability transition pore. A critical appraisal. *J Biol Chem* **272**:12295-12299.

MOL #55277

- Smith ARW, Lambert PA, Hammond SM, and Jessup C (1975) The differing effects of cetyltrimethylammonium bromide and cetrimide B.P. upon growing cultures of *Escherichia coli* NCIB 8277. *J Appl Bacteriol* **38**:143-149.
- Sonisik M, Korkmaz A, Besim H, Karayalcin K, and Hamamci O (1998) Efficacy of cetrimide-chlorhexidine combination in surgery for hydatid cyst. *Br J Surg* **85**:1277.
- Suzuki T, Murakami T, Iino R, Suzuki J, Ono S, Shirakihara Y, and Yoshida M (2003) F0F1-ATPase/synthase is geared to the synthesis mode by conformational rearrangement of epsilon subunit in response to proton motive force and ADP/ATP balance. *J Biol Chem* **278**:46840-46846.
- Umpleby HC, and Williamson RC (1984) The efficacy of agents employed to prevent anastomotic recurrence in colorectal carcinoma. *Ann R Coll Surg Engl* **66**:192-194.
- Wagner BK, Kitami T, Gilbert TJ, Peck D, Ramanathan A, Schreiber SL, Golub TR, and Mootha VK (2008) Large-scale chemical dissection of mitochondrial function. *Nat Biotechnol* **26**:343-351.
- Warburg O (1930) *The Metabolism of Tumours: Investigations from the Kaiser-Wilhelm Institute for Biology*. Constable, London.
- Weiss MJ, Wong JR, Ha CS, Bleday R, Salem RR, Steele GD, Jr., and Chen LB (1987) Dequalinium, a topical antimicrobial agent, displays anticarcinoma activity based on selective mitochondrial accumulation. *Proc Natl Acad Sci U S A* **84**:5444-5448.
- Xu C, Bailly-Maitre B, and Reed JC (2005) Endoplasmic reticulum stress: cell life and death decisions. *J Clin Invest* **115**:2656-2664.

MOL #55277

- Yip KW, Ito E, Mao X, Au PY, Hedley DW, Mocanu JD, Bastianutto C, Schimmer A, and Liu FF (2006a) Potential use of alexidine dihydrochloride as an apoptosis-promoting anticancer agent. *Mol Cancer Ther* **5**:2234-2240.
- Yip KW, Mao X, Au PY, Hedley DW, Chow S, Dalili S, Mocanu JD, Bastianutto C, Schimmer A, and Liu FF (2006b) Benzethonium chloride: a novel anticancer agent identified by using a cell-based small-molecule screen. *Clin Cancer Res* **12**:5557-5569.
- Yip KW, Mocanu JD, Au PY, Sleep GT, Huang D, Busson P, Yeh WC, Gilbert R, O'Sullivan B, Gullane P, Bastianutto C, and Liu FF (2005) Combination bcl-2 antisense and radiation therapy for nasopharyngeal cancer. *Clin Cancer Res* **11**:8131-8144.
- Zhang JH, Chung TD, and Oldenburg KR (1999) A Simple Statistical Parameter for Use in Evaluation and Validation of High Throughput Screening Assays. *J Biomol Screen* **4**:67-73.
- Zips D, Krause M, Hessel F, Westphal J, Bruchner K, Eicheler W, Dorfler A, Grenman R, Petersen C, Haberey M, and Baumann M (2003) Experimental study on different combination schedules of VEGF-receptor inhibitor PTK787/ZK222584 and fractionated irradiation. *Anticancer Res* **23**:3869-3876.

MOL #55277

FOOTNOTES

Financial Support:

This work was supported by the Canadian Institutes of Health Research (Grant 69023) and the Elia Chair in Head and Neck Cancer Research. Emma Ito is a recipient of a Natural Sciences and Engineering Research Council of Canada scholarship.

Reprint Requests:

Dr. Fei-Fei Liu
Department of Radiation Oncology
Ontario Cancer Institute, Princess Margaret Hospital
610 University Avenue, Room 5-983
Toronto, Ontario, Canada M5G 2M9
Email: Fei-Fei.Liu@rmp.uhn.on.ca

FIGURE LEGENDS

Figure 1. Characterization of cetrimonium bromide as a potential anti-cancer agent for HNC. **A**, Chemical structure of CTAB. **B**, Cell viability dose-response curves for CTAB in six cancer (FaDu, C666-1, UTSCC-8A, UTSCC-42A, A549, and MCF7) and two normal (GM05757 and MRC5) cell lines. MTS viability assays were performed 48 h after drug treatment. Line, 50% cell viability (EC_{50}). **C**, Effect of combining CTAB with γ -radiation on the clonogenic survival of FaDu cells. Cells (10^2 – 10^4 per well) were seeded and incubated with increasing concentrations of CTAB for 48 h; where indicated, cells were irradiated 24 h after small-molecule treatment. Ten days later, colonies were counted. Each datum represents the mean \pm SE from at least three independent experiments.

Figure 2. Cetrimonium bromide induces apoptosis in human HNC cells. **A**, Hoechst-33342 staining of CTAB-treated (48 h) FaDu cells revealed condensed chromatin with nuclear blebbing, morphologic indicators of apoptosis, which were absent in GM05757 fibroblasts. Bar, 10 μ m. **B**, Flow cytometric DNA content analyses of CTAB-treated FaDu and C666-1 cells revealed a dramatic increase in the population of cells with subG₁ DNA content, but not in GM05757 fibroblasts. **C**, Fluorescent caspase inhibitor peptide-based assays demonstrated significant CTAB-induced caspase activation in FaDu and C666-1 cells, which increased in a time-dependent manner. Minimal increases in caspase activation were observed in CTAB-treated GM05757 fibroblasts over 12–72 h. **, $P < 0.05$ and *, $P < 0.01$, statistically significant fold differences compared to vehicle control. **D**, Inhibition of caspase activation significantly suppressed CTAB-induced apoptosis. FaDu cells were incubated with or without Z-VAD.FMK (25 μ M; 1 h) prior to CTAB treatment for 24 h. Apoptotic fractions were assessed by flow

cytometry. *, $P < 0.01$, statistically significant difference compared to CTAB alone. Each column represents the mean \pm SE from three independent experiments. In all cases, cells were treated with 5 μ M of CTAB (EC_{75}); vehicle represents sterile H_2O .

Figure 3. Evaluation of cetrimonium bromide-mediated apoptosis. **A**, Transmission electron microscopy was used to visualize the subcellular morphological characteristics of CTAB-induced cytotoxicity in FaDu cells. Chromatin condensation (top; black arrow) and membrane blebbing (top; white arrow), as well as mitochondrial autophagy (middle; arrow) were observed. Rough endoplasmic reticulum (bottom; arrow) appeared to be unaffected. Bar, 1 μ m. **B**, Mitochondria (arrow) of CTAB-treated GM05757 fibroblasts remained intact up to 96 h. Bar, 1 μ m. **C**, FaDu cells treated for 2, 4, 6, or 12 h with CTAB were simultaneously stained with DiIC₁(5) ($\Delta\Psi_M$), indo-1 AM (cytosolic Ca^{2+}), and propidium iodide (PI; membrane integrity/cell viability). Gates for quantification are shown. Box A, mitochondrial membrane potential ($\Delta\Psi_M$) depolarized cells; Box B, $\Delta\Psi_M$ polarized cells; Box C, $\Delta\Psi_M$ depolarized and dead cells; Box D, $\Delta\Psi_M$ depolarized and viable cells; Box E, $\Delta\Psi_M$ polarized and viable cells. Each experiment was performed three independent times. In all cases, cells were treated with 5 μ M of CTAB (EC_{75}); vehicle represents sterile H_2O .

Figure 4. Cetrimonium bromide induces mitochondrial dysfunction. **A**, Effect of CTAB (2.5–50 μ M) on mitochondrial H^+ -ATP synthase activity in FaDu cells. Percent inhibition was calculated by dividing the specific enzyme activity (normalized to protein quantity) of CTAB- vs. vehicle-treated ATPase. *, $P < 0.01$, statistically significant difference compared to untreated cells (ATPase inhibition set as 0%). **B**, GM05757 and FaDu cells were treated with CTAB for 6–96 h

and assessed for changes in intracellular ATP levels. In all cases, cells were treated with 5 μ M of CTAB (EC_{75}). **, $P < 0.05$ and *, $P < 0.01$, statistically significant differences compared to untreated cells (ATP content set as 100%). Each column represents the mean \pm SE from at least three independent experiments.

Figure 5. Role of $\Delta\Psi_M$ in cetrimonium bromide-mediated apoptosis. **A**, Mitochondrial transmembrane potentials of GM05757, MRC5, A549, and FaDu cells. In cells with high $\Delta\Psi_M$, the JC-1 dye forms red fluorescent J-aggregates. JC-1 remains in the green fluorescent monomeric form in cells with low $\Delta\Psi_M$. The ratio of red to green fluorescence serves as a readout for $\Delta\Psi_M$. *, $P < 0.01$, statistically significant difference compared to FaDu cells. **B**, FaDu cells treated with or without CCCP (5 μ M) were stained with DiBAC₄(3) and DiIC₁(5) to measure relative changes in $\Delta\Psi_P$ and $\Delta\Psi_M$, respectively. **, $P < 0.05$, statistically significant fold difference compared to untreated cells. **C**, Effect of $\Delta\Psi_M$ on CTAB-mediated cytotoxicity. FaDu cells were incubated in medium with or without CCCP (5 μ M; 1 h) prior to CTAB treatment (5 μ M) for 24 h. SubG₁ apoptotic fractions were assessed by flow cytometry. **, $P < 0.05$, statistically significant difference compared to CTAB alone. **D**, Effect of $\Delta\Psi_M$ on oligomycin-mediated cytotoxicity. FaDu cells were incubated in medium \pm CCCP (5 μ M; 1 h) prior to oligomycin (OLIG) treatment (30 μ M; EC_{75}) for 48 h. SubG₁ apoptotic fractions were assessed by flow cytometry. **E**, Cell viability dose-response curves for oligomycin in four cancer (FaDu, C666-1, A549, and MCF7) cell lines. MTS assays were performed 48 h after drug treatment. Line, 50% cell viability (EC_{50}). **F**, FaDu cells pre-incubated in medium \pm nigericin (5 or 10 nM; 1 h) prior to CTAB treatment (5 μ M; 24 h) were assessed for apoptosis *via* flow cytometry. Each datum represents the mean \pm SE from at least two independent experiments.

MOL #55277

Figure 6. *In vivo* efficacy of cetrimonium bromide. **A**, FaDu cells treated with vehicle (H₂O) or CTAB (5 μ M) for 48 h were injected into the left gastrocnemius muscle of SCID mice. CTAB-treated cells did not form tumors even after 100 days. **B**, FaDu xenograft tumors were established in SCID mice; once the tumor-plus-leg diameters (TLD) reached 7.5 mm, the mice were randomly allocated to one of the following groups: vehicle, CTAB, local radiation therapy (RT)-plus-vehicle, or RT-plus-CTAB. The mice were administered one i.p. injection (5 mg/kg) daily of either vehicle (H₂O) or drug for five consecutive days. Local tumor RT (4 Gy) was delivered on days 2 and 5 before the i.p. injections. The mice were euthanized once TLDs reached 14 mm. Solid line, mean time to reach a TLD of 14 mm. *, $P < 0.05$, statistically significant difference between CTAB *vs.* vehicle or RT-plus-CTAB *vs.* RT-plus-vehicle. **C**, Total body weight was also recorded for each group, demonstrating no significant difference. Each datum represents the mean \pm SE from three independent experiments (3 mice/treatment group/experiment).

Figure 7. Anti-cancer efficacy of cetrimonium bromide analogues. **A**, Chemical structures of CTAB, cetyltrimethylammonium chloride (analogue 1), dodecyltrimethylammonium bromide (analogue 2), hexyltrimethylammonium bromide (analogue 3), tetramethylammonium bromide (analogue 4), and butyltriethylammonium bromide (analogue 5). **B**, Cell viability dose-response curves for CTAB and analogues 1–5 in FaDu cells. **C**, Dose-response curves for CTAB and analogues in GM05757 fibroblasts. Line, 50% cell viability (EC_{50}). Only analogues 1 and 2 retained selective anti-cancer cytotoxicity and bioactivity with EC_{50} values similar to CTAB. MTS viability assays were performed 48 h after drug treatment. Each datum represents the mean \pm SE from three independent experiments.

TABLES

Table 1. HTS of the Spectrum Collection small molecule library for novel HNC cytotoxics. Eighteen compounds were identified with preferential toxicity against FaDu cells. Percent inhibition of FaDu cell viability induced by each compound is shown. Validity of the screen was corroborated by the identification of existing chemotherapeutic agents such as novantrone, dactinomycin, and mechlorethamine.

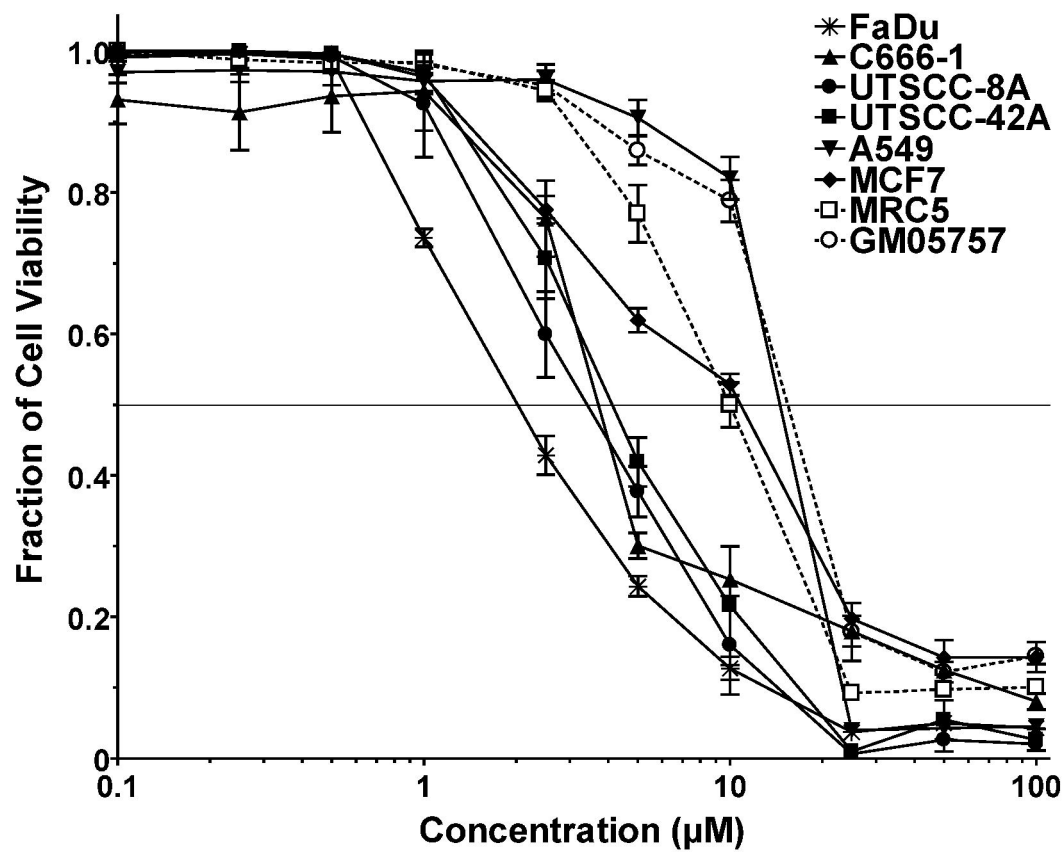
Compound	Molecular Formula	Inhibition (%)
Mitoxantrone Hydrochloride	C ₂₂ H ₃₀ Cl ₂ N ₄ O ₆	100
Mitomycin C	C ₁₅ H ₁₈ N ₄ O ₅	96
Mechlorethamine	C ₅ H ₁₁ Cl ₂ N	91
Antimycin A	C ₂₈ H ₄₀ N ₂ O ₉	91
Deguelin	C ₂₃ H ₂₂ O ₆	90
Camptothecin	C ₂₀ H ₁₆ N ₂ O ₄	89
Beta-Dihydrorotenone	C ₂₃ H ₂₄ O ₆	88
10-Hydroxycamptothecin	C ₂₀ H ₁₆ N ₂ O ₅	87
Actinomycin D	C ₆₂ H ₈₆ N ₁₂ O ₁₆	87
Dihydrorotenone	C ₂₃ H ₂₄ O ₆	85
Aklavin Hydrochloride	C ₃₀ H ₃₆ ClNO ₁₀	82
Pyrromycin	C ₃₀ H ₃₅ NO ₁₁	80
Teniposide	C ₃₂ H ₃₂ O ₁₃ S	76
Floxuridine	C ₉ H ₁₁ FN ₂ O ₅	72
Cetrimonium Bromide	C ₁₉ H ₄₂ BrN	71
Alexidine Dihydrochloride	C ₂₆ H ₅₇ ClN ₁₀	60
Benzethonium Chloride	C ₂₇ H ₄₂ ClNO ₂	57
Aminopterin	C ₁₉ H ₂₀ N ₈ O ₅	51

Figure 1

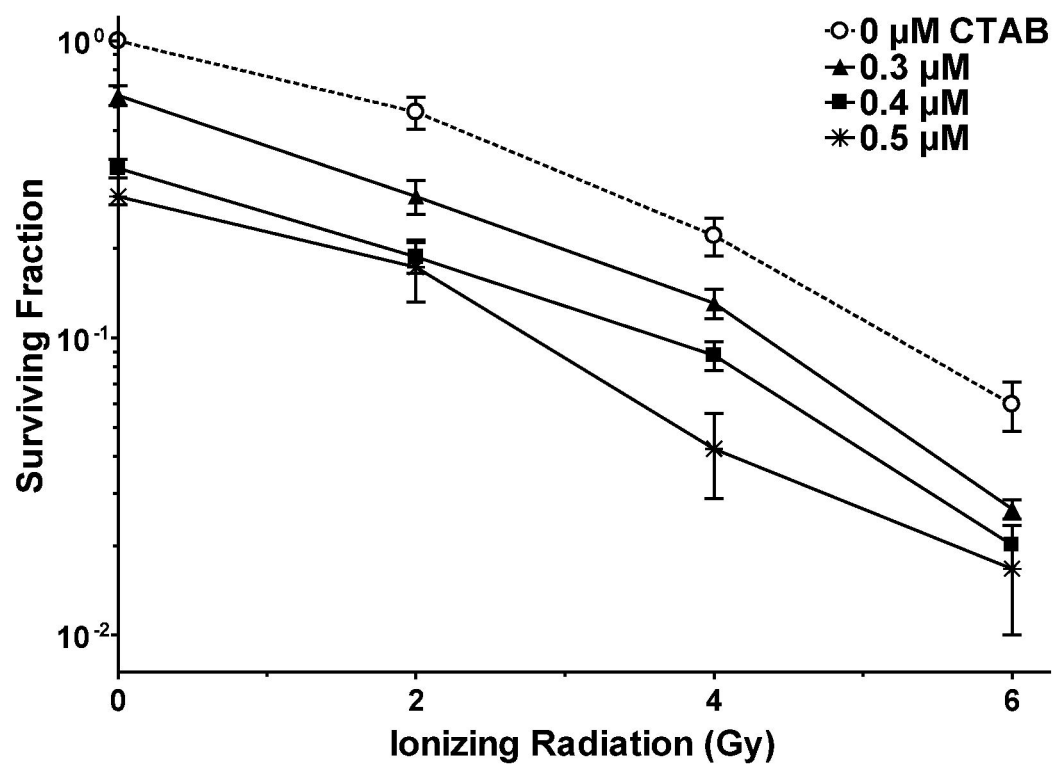
A



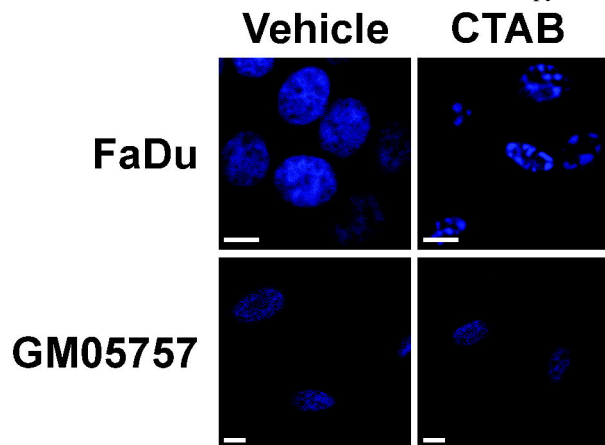
B



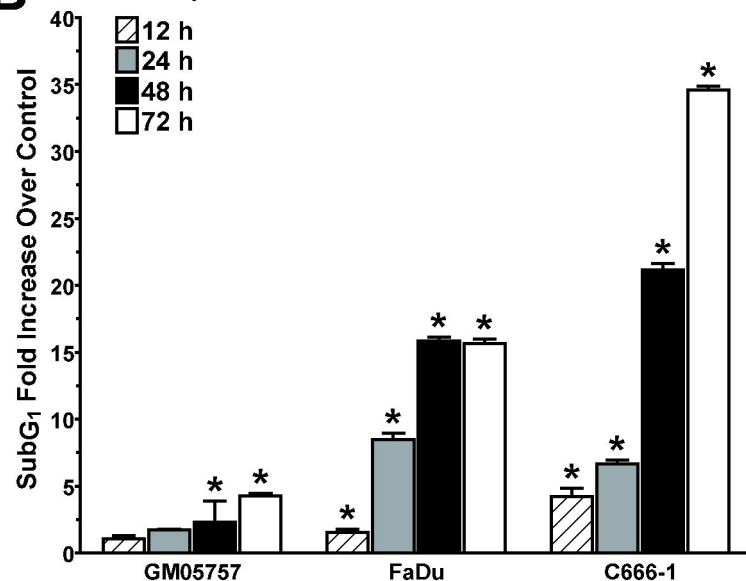
C



A

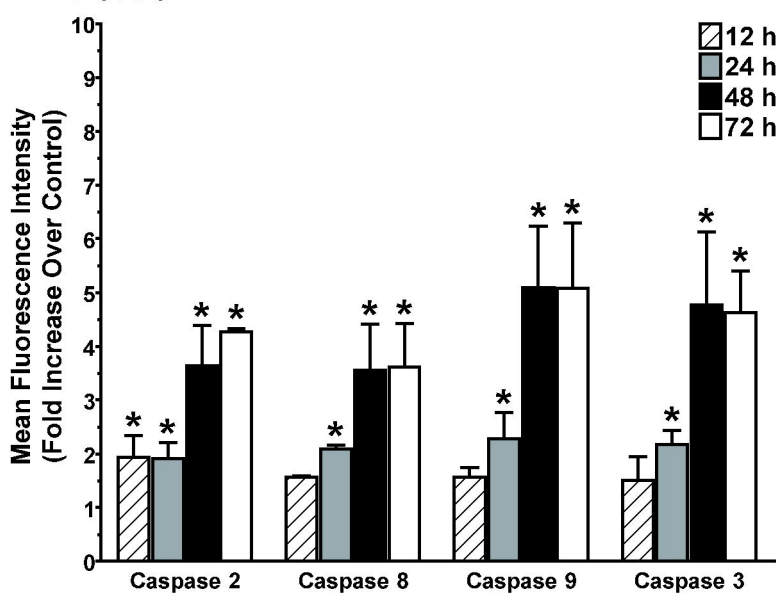


B

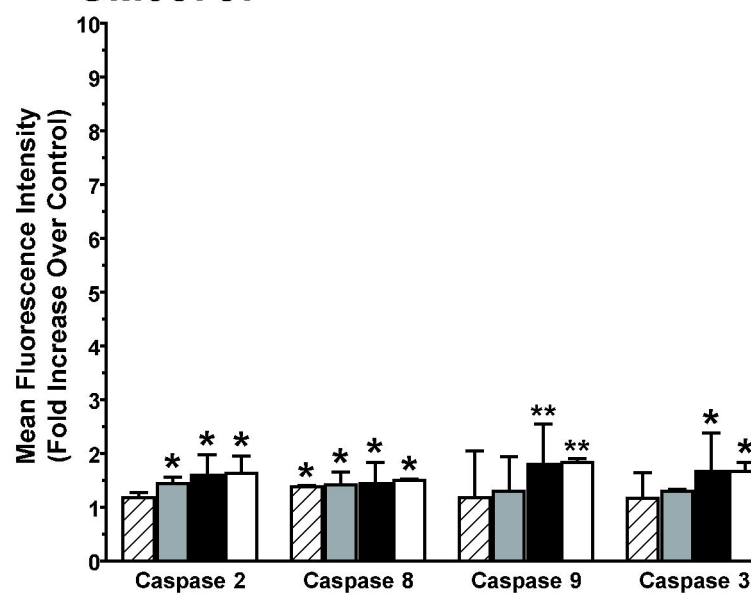


C

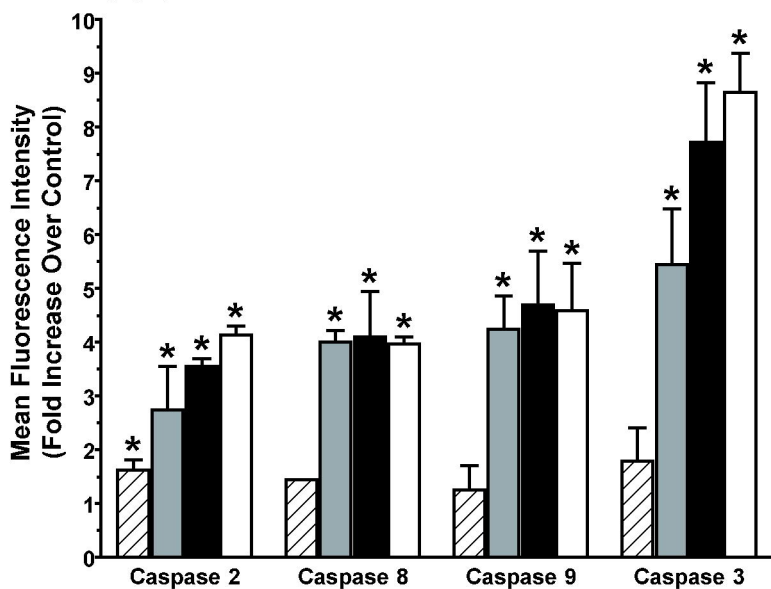
FaDu



GM05757



C666-1



D

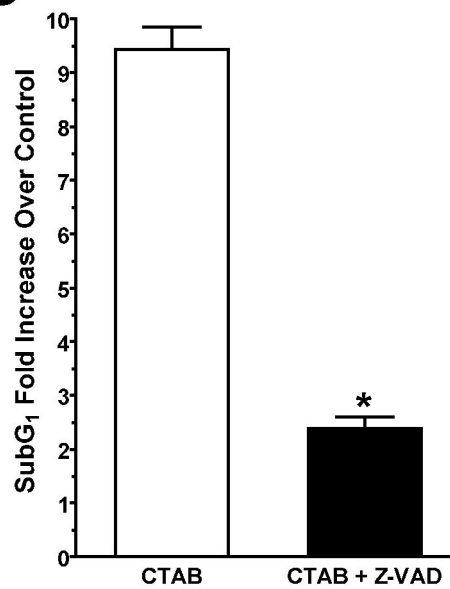


Figure 2

Figure 3

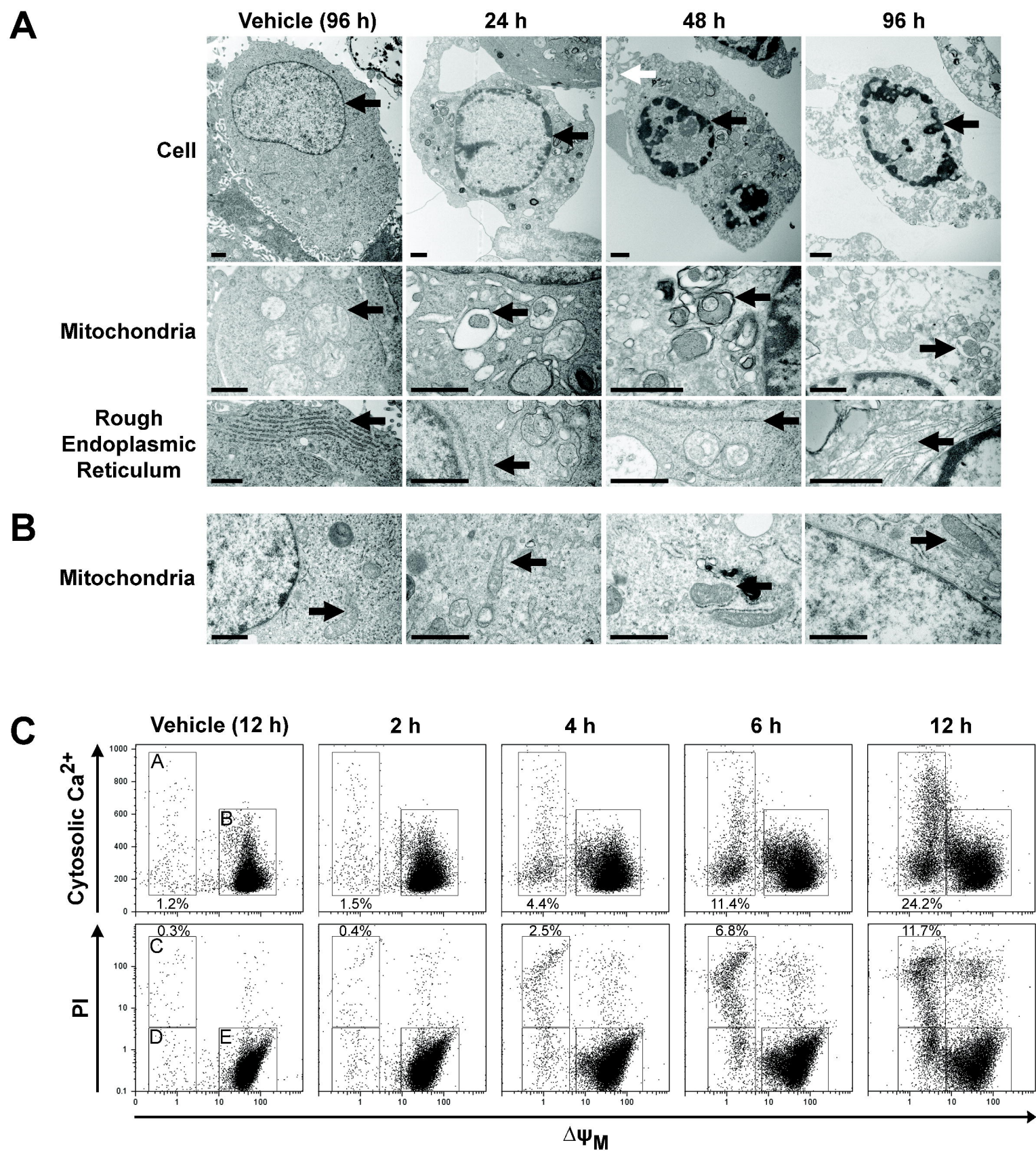
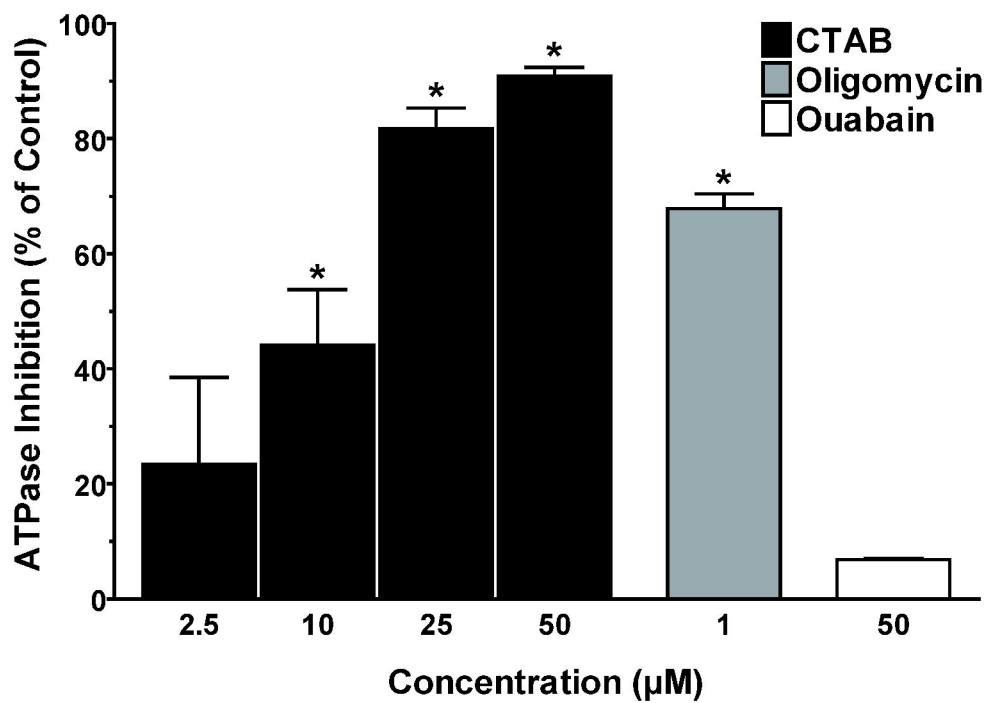
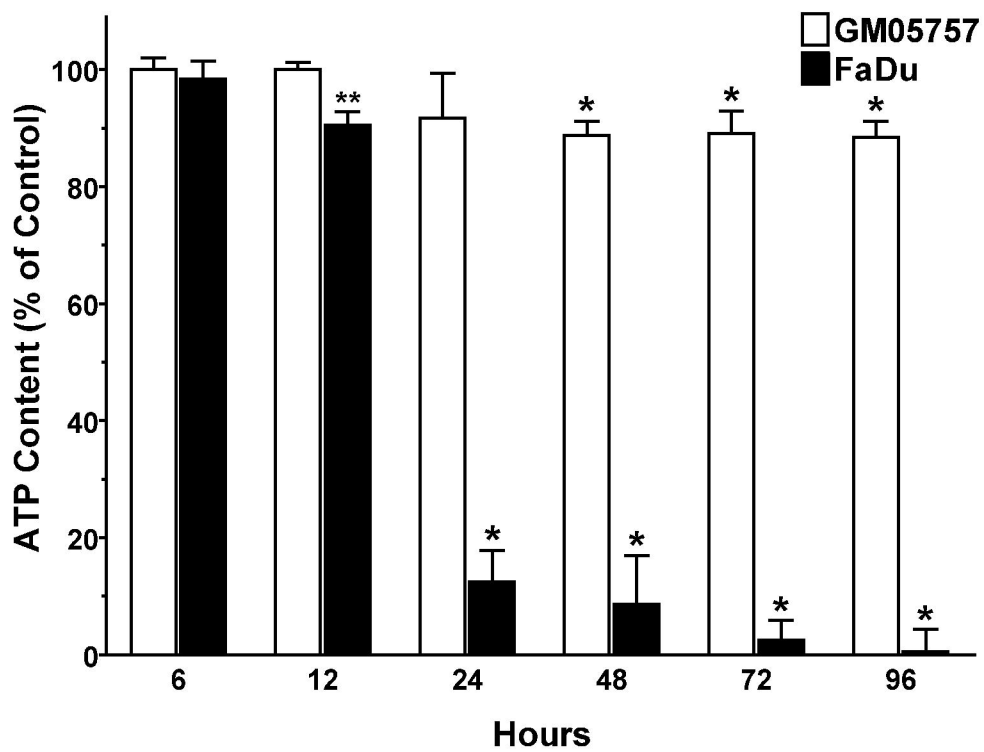


Figure 4

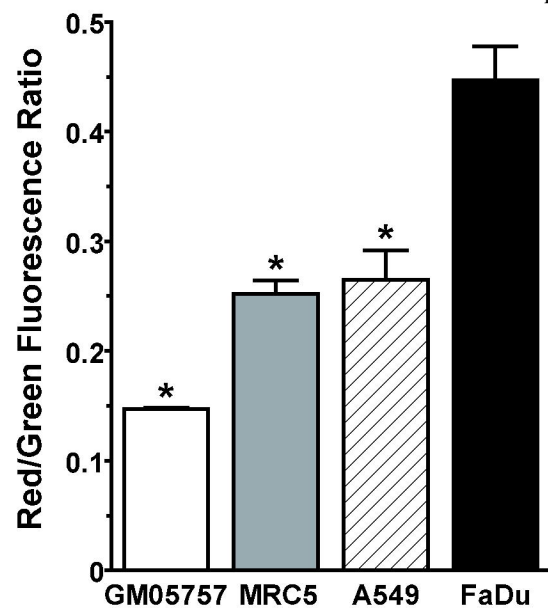
A



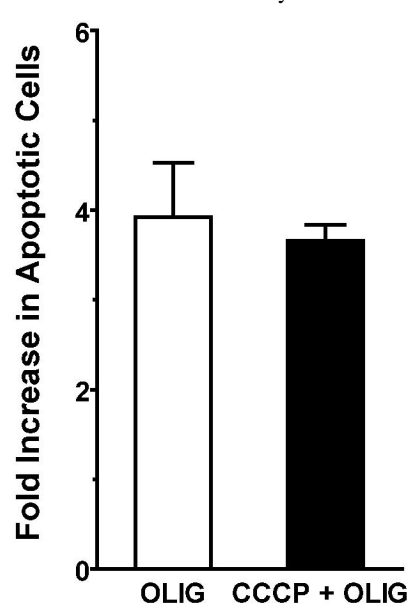
B



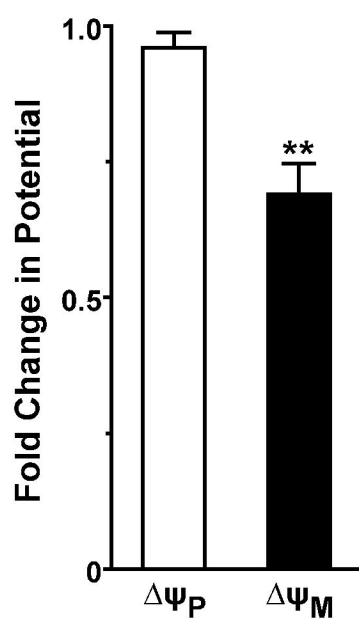
A



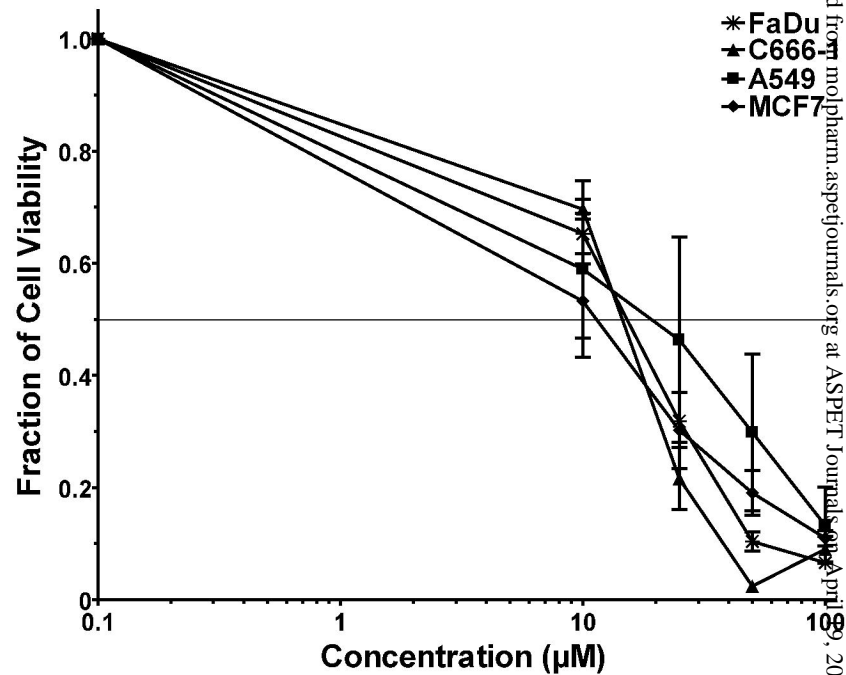
D



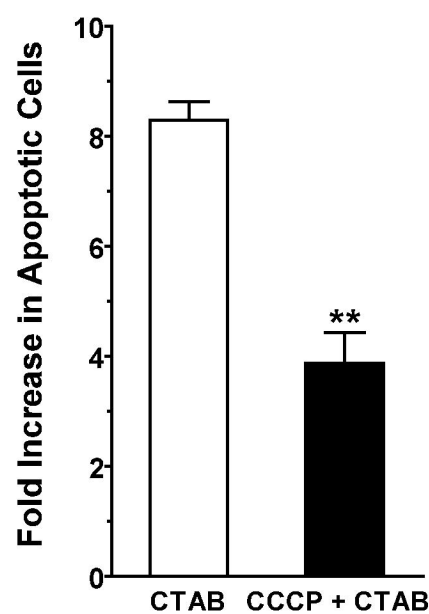
B



E



C



F

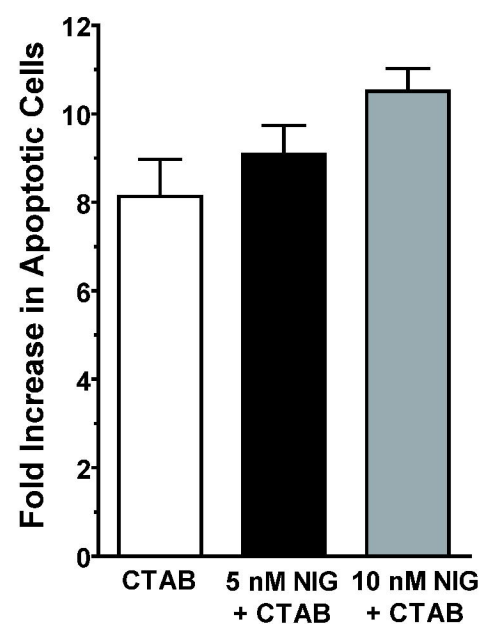


Figure 6

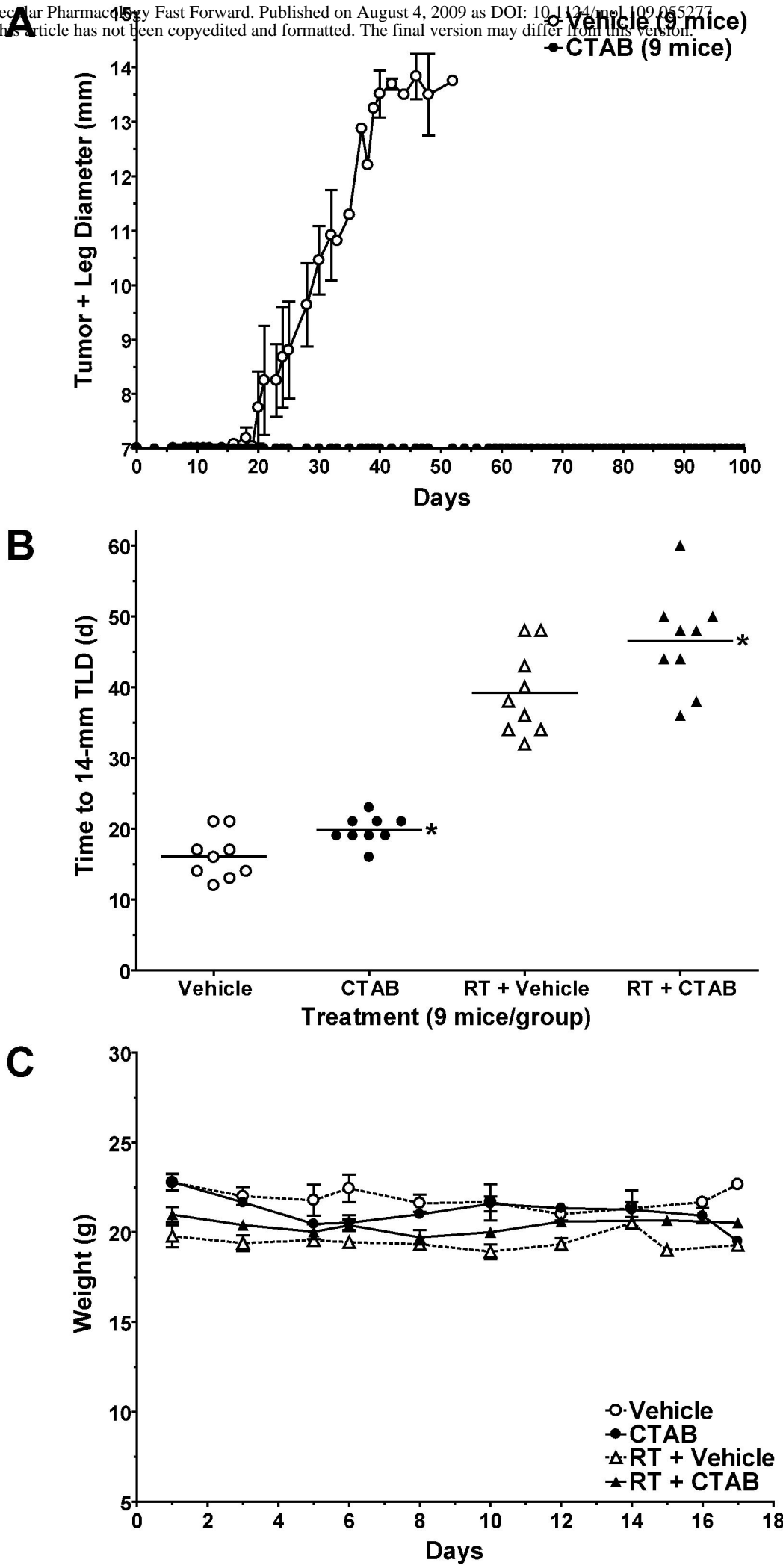


Figure 7

